ACS APPLIED NANO MATERIALS

www.acsanm.org Article

DNA Binding on Self-Assembled Monolayers Terminated with Mixtures of Ammonium and Trimethylammonium Groups: Toward a Gene-Delivery Platform

Johnson Hoang, Chul Soon Park, Maria D. Marquez, Preethi H. Gunaratne,* and T. Randall Lee*

Cite This: *ACS Appl. Nano Mater.* 2020, 3, 6621−6628 Read Online

ACCESS | Metrics & More | Article Recommendations | Supporting Information

ABSTRACT: The formation of binary self-assembled monolayers (SAMs) via the use of ammonium-terminated adsorbates offers an ionic platform for the binding of oligonucleotides and their subsequent delivery for therapeutic applications. Four different types of ammonium-terminated adsorbates were used in the present study: two ammonium-terminated and two trimethylammonium-terminated dithiols of different chain lengths, which were designed to provide a foundation for the development of a high-capacity nanoscale loading system for oligonucleotides. The maximum number of oligonucleotides immobilized on the surface was achieved by adjusting the ratio of the adsorbates in correlation with the relative packing density of the SAMs. The techniques of ellipsometry, X-ray photoelectron spectroscopy, polarization modulation infrared reflection-absorption spectroscopy, and electrochemical quartz crystal microbalance were used to analyze the SAMs. Analysis of the films revealed an optimum ratio of 75:25 of the long-chained adsorbate (ammonium-terminated) to the short-chained adsorbate (trimethylammonium-terminated) for maximum oligonucleotide loading. Further analysis indicated that burying the trimethylammonium termini into the lower interface of the monolayer provided the highest mass loading of oligonucleotides. The results presented in this study provide a foundation for the development of a gene-therapy platform when constructed on the surface of, for example, light-responsive gold nanoparticles or gold nanoshells as photo-triggerable delivery vehicles.

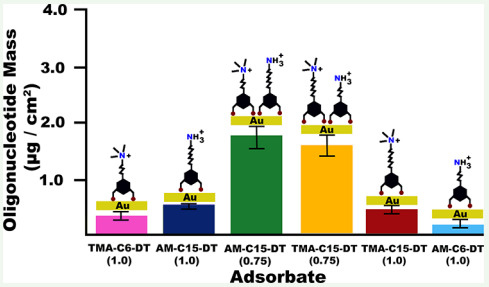

KEYWORDS: *ammonium, trimethylammonium, binary-mixed SAMs, oligonucleotide delivery, single-stranded DNA*

INTRODUCTION

Self-assembled monolayers (SAMs) derived from organosulfur adsorbates having terminal cationic ammonium groups have been extensively studied, yielding many practical developments that include the immobilization of biomolecules,[1,2] protein chips,[2,3] and microarrays.[4,5] SAMs have become a prominent integration platform for multiple applications due to their ease of use and versatility, which allows for their formation on a variety of metallic substrates (e.g., gold, silver, palladium, copper, and platinum).[6] Furthermore, the immobilization of adsorbates on selected substrates depends on the nature of the headgroup (e.g., thiols, silanes, and phosphonates),[6,7] which enables the spontaneous formation of the monolayer via chemisorption. The adsorbate terminal groups can be tailored to incorporate a variety of moieties to impart specific properties to a film; examples of terminal groups that have significant interactions with biological species such as proteins,[6,8−10] enzymes,[6,10] and oligonucleotide base systems (e.g., microRNA, small interfering RNA, single-stranded DNA, and double-stranded DNA),[6,11,12] include amine, azide, and carboxylic acids.[6,13,14]

Oligonucleotides play important roles in applied SAMs research due to their activity in post-transcriptional regulation.[15−17] However, chemical modification of oligonucleotides to induce covalent bonding to substrates can interfere with the functionality of the oligonucleotide, which can give rise to off-target effects.[18] Furthermore, since dissociation of oligonucleotides from the SAM surface is a vital step for gene delivery, covalent bonding renders it difficult to dissociate the oligonucleotides from the surface, hindering the functional prevalence of their usage for gene therapy. As an alternative method, the use of ionic bonds, via the use of charged termini, to attach oligonucleotides on surfaces can plausibly provide efficient delivery systems.[19] Additionally, the physical adsorption of oligonucleotides offers ease of dissociation from the complex through external methods such as pH adjustment[20] or light induction.[21] Successful attachment of unmodified oligonucleotides on charged surfaces, such as ammonium- and trimethylammonium-terminated SAMs, through ionic bonds has been demonstrated.[21−28] Furthermore, ammo-

Received: April 20, 2020
Accepted: June 11, 2020
Published: June 11, 2020

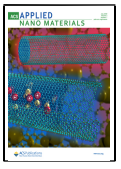

https://dx.doi.org/10.1021/acsanm.0c01059
ACS Appl. Nano Mater. 2020, 3, 6621−6628

nium-terminated adsorbates can form hydrogen bonds with the carbonyl group of the nucleotides to the ammonium group of the SAMs.[29] However, the dominant adsorption force is the electrostatic interaction between the phosphate backbone of the oligonucleotides and the ammonium group.[20,30] Importantly, we noted previously that the trimethylammonium termini in these types of SAMs give rise to an increase in the lateral spacing of the chains, exposing the aliphatic spacer of the adsorbate and allowing the intercalation of biomolecules into the film and increase in the loading capacity of biomolecules on the surface.[26]

Moreover, SAMs derived from bidentate thiol-based adsorbates have been shown to generate monolayer films having loosely packed terminal chains;[25,31,32] as such, the use of binary SAMs enables further capacity to manipulate the packing density of SAMs on gold for enhanced oligonucleotide binding.[26] While decreasing the chain packing density of SAMs can allow biomolecules to intercalate into the loosely packed film, the biomolecules will be only weakly associated with the chains in the film and can be easily released.[26]

In an effort to circumvent the aforementioned shortcomings, we recently demonstrated the use of positively charged quaternary ammonium binary SAMs for high-capacity loading of negatively charged oligonucleotides on the surface of the SAMs (i.e., oligonucleotide immobilization via electrostatic attraction).[26] We envision that such immobilization on Au nanoparticles or nanoshells will inhibit degradation of the oligonucleotides by nucleases or lysosomes.[33−37] The most widely accepted endosomal delivery or "escape" mechanism hypothesizes that the influx of protons through the Vacuolar-type H^+-ATPase (V-ATPase) into the lysosome compartment initiates the protonation of unprotonated amines.[35,36] Protonation then gives rise to a passive influx of chloride ions into the endosome, which causes osmotic swelling of the endosome and consequently leads to the release of the nanomaterials into the cytosol.[34,36,38] Given these considerations, we utilize in the present study four different SAM adsorbates having selectively distinct chain lengths and an ammonium or trimethylammonium terminal group (see Figure 1): 15-(3,5-bis-

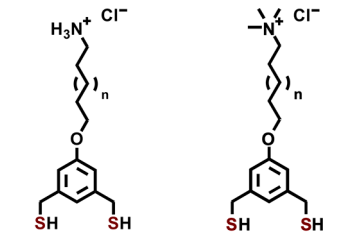

Figure 1. Molecular structures of the ammonium-terminated adsorbates (**AM-C6-DT** and **AM-C15-DT**) and the trimethylammonium-terminated adsorbates (**TMA-C6-DT** and **TMA-C15-DT**) used to generate SAMs.

(mercaptomethyl)phenoxy)penta-decan-1-aminium (**AM-C15-DT**), 15-(3,5-bis(mercaptomethyl)phenoxy)-*N*,*N*,*N*-trimethylpenta-decan-1-aminium (**TMA-C15-DT**), 6-(3,5-bis-(mercaptomethyl)phenoxy)hexan-1-aminium (**TMA-C6-DT**), and 6-(3,5-bis(mercaptomethyl)phenoxy)-*N*,*N*,*N*-trimethylhexan-1-aminium (**AM-C6-DT**). We have also included octadecanethiol (**ODT**) in the study for generating a standard SAM for comparison.

Our study explores the composition, structure, and properties of two series of binary SAMs derived from various solution ratios of the adsorbates shown in Figure 1. Specifically, the two series consist of mixtures of the **AM-C15-DT** and **TMA-C6-DT** adsorbates (the "**AM** Series") and mixtures of the **TMA-C15-DT** and **AM-C6-DT** adsorbates (the "**TMA** Series"). We chose these specific combinations because our initial studies of TMA-based SAMs found that 50:50 ratios of **TMA-C6-DT** and **TMA-C15-DT** showed the greatest oligonucleotide binding.[26] With this systematic approach, we aim to elucidate the structural features of the SAMs that have meaningful impacts on oligonucleotide loading based on the following: (1) the type of terminal group used (i.e., ammonium-terminated or trimethylammonium-terminated); (2) the length of the aliphatic spacer of the adsorbate; and (3) the packing density of the films. The development and understanding of these SAMs can provide key insights into further development of transfection delivery systems in which the covalent bonding between oligonucleotides and nanoparticles can provide a platform for sequestering the degradation of oligonucleotides to prevent degradation and enhance the delivery of the gene payloads into cells.[24]

EXPERIMENTAL SECTION

The Supporting Information provides a detailed description of the materials, methods, instrumentation, and synthetic procedures used to synthesize the adsorbates according to Scheme S1. The Supporting Information also provides a comprehensive characterization of the adsorbates [(**AM-C15-DT**, **AM-C6-DT**, **TMA-C15-DT**, and **TMA-C6-DT**)] using ^{1}H NMR spectroscopy, ^{13}C NMR spectroscopy, and high-resolution mass spectrometry (see Figures S1−S4), along with a description of the material and methods for forming SAMs using different molar ratios of adsorbates (see Tables S1 and S2). The conjugation of the SAMs with single-stranded DNA (ssDNA) was performed as described previously[26] and is summarized again briefly in the Supporting Information.

RESULTS AND DISCUSSION

Binary Self-Assembled Monolayer Films Derived from Various Ratios of Ammonium- and Trimethylammonium-Terminated Adsorbates. *Measurements of Film Thickness.* Chemisorption of the adsorbates on the gold substrate was initially verified using ellipsometry to determine the film thickness. As shown in Table 1, the average

Table 1. Ellipsometric Thicknesses of SAMs Derived from ODT, the AM Series (AM-C15-DT/TMA-C6-DT), and the TMA series (TMA-C15-DT/AM-C6-DT)[a]

AM series		TMA series	
adsorbate	film thickness (Å)	adsorbate	film thickness (Å)
ODT	23 ± 1	**ODT**	23 ± 1
AM-C15-DT (1.0)	21 ± 1	**TMA-C15-DT** (1.0)	22 ± 1
AM-C15-DT (0.75)	19 ± 1	**TMA-C15-DT** (0.75)	20 ± 1
AM-C15-DT (0.50)	17 ± 1	**TMA-C15-DT** (0.50)	17 ± 1
AM-C15-DT (0.25)	16 ± 1	**TMA-C15-DT** (0.25)	16 ± 1
TMA-C6-DT (1.0)	14 ± 1	**AM-C6-DT** (1.0)	13 ± 1

[a]The mole fraction of the adsorbate in the solution is denoted inside the parentheses.

https://dx.doi.org/10.1021/acsanm.0c01059
ACS Appl. Nano Mater. 2020, 3, 6621−6628

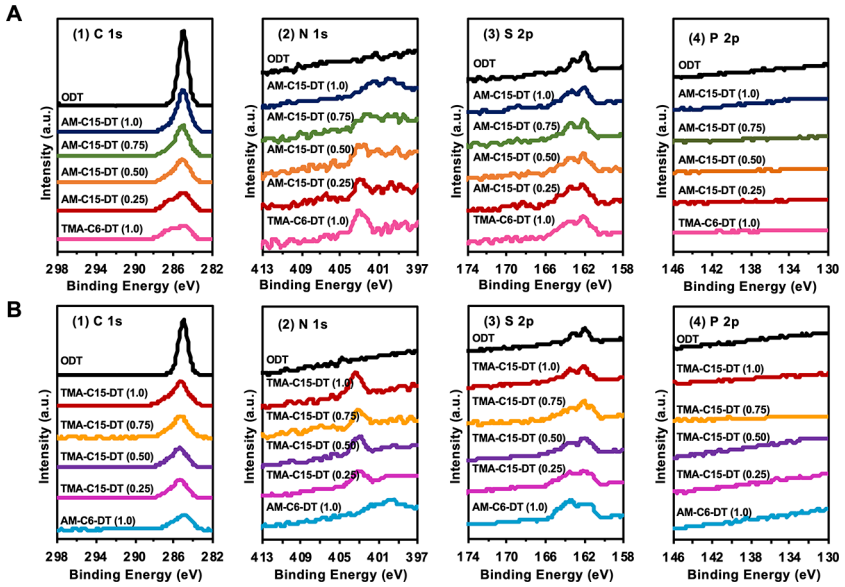

Figure 2. XPS spectra of (A) the **AM** series and (B) the **TMA** series for the (1) C 1s, (2) N 1s, (3) S 2p, and (4) P 2p regions. The SAMs derived from **ODT** are included in both panels for comparison.

thicknesses of the single-component SAMs generated from **ODT**, **AM-C15-DT** (1.0), **AM-C6-DT** (1.0), **TMA-C15-DT** (1.0), and **TMA-C6-DT** (1.0) were 23, 21, 13, 22, and 14 Å, respectively. The thicknesses of the single-component SAMs derived from **ODT**, **TMA-C15-DT**, and **TMA-C6-DT** are in agreement with previously reported values, which lends credibility to the results obtained from the newly generated SAMs.[26] Furthermore, the single-component SAMs generated from the ammonium-terminated adsorbates (**AM-C15-DT** and **AM-C6-DT**) exhibited film thicknesses consistent with the TMA-terminated analogs and other similarly structured adsorbates.[25,39] Notably, the single-component SAMs derived from the short-chain analogs, **AM-C6-DT** and **TMA-C6-DT**, were thinner by ∼8 Å than their long-chain analogs, **AM-C15-DT** and **TMA-C15-DT**, which can be attributed to the shorter length of the hydrocarbon chain linking the aromatic ring to the ammonium or trimethylammonium terminal group, respectively.

The two-component binary SAMs were generated from specific ratios of the adsorbates, and the corresponding film thicknesses are also shown in Table 1. Film thickness values obtained from the SAMs generated from the AM series **AM-C15-DT** (0.75), **AM-C15-DT** (0.50), and **AM-C15-DT** (0.25) mixed with complementary amounts of **TMA-C6-DT** were 19, 17, and 16 Å, respectively. Separately, monolayers generated by mixing the TMA series **TMA-C15-DT** (0.75), **TMA-C15-DT** (0.50), and **TMA-C15-DT** (0.25) with complementary amounts of **AM-C6-DT** exhibited film thickness values of 20, 17, and 16 Å, respectively. These results show that the thickness of the binary SAMs decreases as the ratio of the short-chain adsorbates (**TMA-C6-DT** and **AM-C6-DT**) in the **AM** and **TMA** series, respectively, is increased. This decrease in film thickness corresponds to a decrease in the relative chain packing density in these films, which arises from the introduction of the shorter adsorbate into the film (vide infra). Furthermore, it is plausible that the upper interface of the binary SAMs forms a more disordered film with the introduction of the shorter adsorbate (i.e., a fluidlike structure).[40] Overall, the obtained thickness values for the **AM** series indicate that **AM-C15-DT** (1.0) > **AM-C15-DT** (0.75) > **AM-C15-DT** (0.50) > **AM-C15-DT** (0.25) > **TMA-C6-DT** (1.0). The thickness values obtained for the **TMA** series indicate similar results: **TMA-C15-DT** (1.0) > **TMA-C15-DT** (0.75) > **TMA-C15-DT** (0.50) > **TMA-C15-DT** (0.25) > **AM-C6-DT** (1.0).

Analysis of the AM and TMA Series by X-ray Photoelectron Spectroscopy (XPS). X-ray photoelectron spectroscopy can provide vital information regarding the elemental composition of a surface, the oxidation state of the atoms present within the sample, and the relative packing density of a SAM.[41] All films in the study were analyzed with XPS, and the high-resolution spectra of the S 2p, C 1s, N 1s, and P 2p regions are provided in Figure 2 for the **AM** (Figure 2a) and **TMA** (Figure 2b) series. For these studies, the binding energy of the Au $4f_{7/2}$ electrons was adjusted to 84.0 eV in all of the spectra as a standard for all of the samples (see Figure S5).

The analysis of the C 1s region of the SAMs (Figure 2a1,b1) shows the presence of C−H carbons at ∼285 eV, while the protruding shoulder at ∼286 eV and the peak at ∼286.6 eV correspond to the C−N and C−O carbons, respectively.[22,42] Separately, the peak located at ∼403 eV in the N 1s spectra (Figure 2a2,b2) can be attributed to the nitrogen of the trimethylammonium termini of the **TMA-C15-DT** and **TMA-C6-DT** adsorbates.[22] Additionally, the presence of the ammonium termini of the **AM-C15-DT** and **AM-C6-DT** can be confirmed by the peaks located at ∼401 and 398 eV in the N 1s region, which can be attributed to the protonated and unprotonated amines, respectively.[42]

The S 2p region (Figure 2a3,b3) shows the presence of bound thiolates, with the S 2p peak appearing as a doublet, S $2p_{3/2}$ and S $2p_{1/2}$, at ∼162 eV; for a bound thiolate, the S $2p_{3/2}$ peak appears at a binding energy of ∼ 162 eV, while the S $2p_{1/2}$ peak appears at 163.2 eV.[43−45] Separately, for an unbound thiol, the S $2p_{3/2}$ peak appears at ∼164−165 eV, while an oxidized sulfur species will produce a S $2p_{3/2}$ peak at ∼166−168 eV.[43−45] Further analysis of the S 2p region can provide a vital insight into the percentage of bound thiol. The amount of bound thiol on the gold substrate was determined by

https://dx.doi.org/10.1021/acsanm.0c01059
ACS Appl. Nano Mater. 2020, 3, 6621−6628

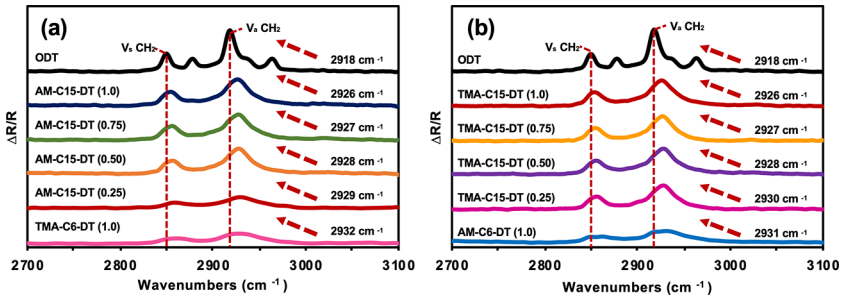

Figure 3. PM-IRRAS spectra of the C−H stretching region for the (a) **AM** series and (b) **TMA** series. The reference SAM derived from **ODT** is included in both panels for comparison.

deconvoluting the S 2p peak. For the **AM** series (Figure S6 and Table S3), the percentages of bound thiol present in the **AM-C15-DT** (1.0), **AM-C15-DT** (0.75), **AM-C15-DT** (0.50), **AM-C15-DT** (0.25), and **TMA-C6-DT** (1.0) samples were 46, 44, 40, 34, and 32%, respectively. Comparatively, in the **TMA** series (Figure S7 and Table S4), the percentages of bound thiol present in the **TMA-C15-DT** (1.0), **TMA-C15-DT** (0.75), **TMA-C15-DT** (0.50), **TMA-C15-DT** (0.25), and **AM-C6-DT** (1.0) samples were 47, 45, 39, 33, and 28%, respectively. Noticeably, as the concentration of the longer adsorbate (**TMA-C15-DT** and **AM-C15-DT**) was lowered and the concentration of the shorter adsorbate (**TMA-C6-DT** and **AM-C6-DT**) increased, a decrease in the amount of bound thiol was observed in both series. Apparent from the data, the mixed SAMs are composed of adsorbates in which one or both thiols are bound to the gold substrate. Incomplete binding in the SAMs is likely driven in part by the large lateral spacing arising from the bulky ammonium termini.[22] Another contribution to the diminished amount of bound thiol can be attributed to the weakened van der Waals (vdW) interactions between the alkyl chains with the introduction of the shorter component, which leads to SAMs with little or no interchain stabilization.[6]

Further analysis of the S 2p region allows for a quantitative analysis of the packing densities (Tables S3 and S4). In particular, the integrated areas of the S 2p and Au 4f peaks have been frequently used to derive sulfur-to-gold (S/Au) ratios to compare the relative packing density of SAMs.[31,46] In our packing density analysis, the SAMs derived from **ODT** were used as a reference (i.e., 100% packing density). According to our results, in the **AM** series, **AM-C15-DT** (1.0), **AM-C15-DT** (0.75), **AM-C15-DT** (0.50), **AM-C15-DT** (0.25), and **TMA-C6-DT** (1.0) exhibited a packing density of 46, 44, 40, 34, and 32%, respectively. Comparatively, in the **TMA** series, **TMA-C15-DT** (1.0), **TMA-C15-DT** (0.75), **TMA-C15-DT** (0.50), **TMA-C15-DT** (0.25), and **AM-C6-DT** (1.0) exhibited a packing density of 47, 45, 39, 33, and 28%, respectively. The packing density analysis revealed a decreasing trend as the concentration of the shorter adsorbate was increased in the mixed SAMs. The decrease in the packing density within the mixed SAMs can be attributed to the presence of the sterically demanding ammonium or trimethylammonium terminal group within the monolayer.[26] We also note that the single-component ammonium-terminated SAMs [**AM-C15-DT** (1.0) and **AM-C6-DT** (1.0)] exhibited a relatively lower packing density compared to the single-component trimethylammonium-terminated SAMs [**TMA-C15-DT** (1.0) and **TMA-C6-DT** (1.0)], suggesting perhaps that the ammonium tailgroups and associated water molecules are more sterically demanding than the more hydrophobic trimethylammonium tailgroups in these single-component SAMs. In additional XPS analyses, the P 2p region (Figure 2a4,b4) fails to show any peaks for phosphorus in the samples, in accordance with the lack of exposure of these surfaces to oligonucleotides.

Analysis of the AM and TMA Series by Polarization Modulation Infrared Reflection-Adsorption (PM-IRRAS). Analysis of the C−H stretching region of a SAM by PM-IRRAS offers valuable insight into the conformational order of the film: specifically, the position of the symmetric ($\nu_s^{CH_2}$) and antisymmetric ($\nu_a^{CH_2}$) C−H stretches of the methylene units. The PM-IRRAS spectra for the **AM** and **TMA** series are provided in Figure 3. A well-ordered film with the alkyl chains in the mostly trans-extended conformation will exhibit a $\nu_a^{CH_2}$ stretch at 2918 cm^{-1}, with shifts to a higher wavenumber indicating a disordered film.[47,48] The $\nu_a^{CH_2}$ stretch of the reference film, **ODT**, appears at 2918 cm^{-1} and is in accordance with the literature.[25,31,48] Examination of the single-component SAMs in both series reveals that the SAM derived from **AM-C15-DT** forms a more conformationally ordered film than the SAM derived from the shorter congener, **AM-C6-DT**, with $\nu_a^{CH_2}$ stretches at 2926 and 2931 cm^{-1}, respectively. A similar trend is observed in the **TMA** series, where the SAM derived from **TMA-C15-DT** has a higher degree of conformational order than the SAM derived from **TMA-C6-DT**, with $\nu_a^{CH_2}$ stretches at 2926 and 2932 cm^{-1}, respectively.[26]

In the **AM** series, the addition of **TMA-C6-DT** into the film produced a more disordered surface when compared to the single-component **AM-C15-DT** SAM. Additionally, there is a systematic decrease in the conformational order of the films in the **AM** series as the concentration of **TMA-C6-DT** is increased, as shown in Figure 3a. The $\nu_a^{CH_2}$ values for the **AM-C15-DT** (0.75), **AM-C15-DT** (0.50), and **AM-C15-DT** (0.25) SAMs show a systematic decrease in the conformational order of the film with values of 2927, 2928, and 2929 cm^{-1}, respectively. Similarly, in the **TMA** series, the degree of conformational order of the mixed SAMs decreased as the concentration of the **AM-C6-DT** adsorbate was increased (Figure 3b); the $\nu_a^{CH_2}$ values for **TMA-C15-DT** (0.75), **TMA-C15-DT** (0.50), and **TMA-C15-DT** (0.25) were 2927, 2928, and 2930 cm^{-1}, respectively. It is likely that the introduction of the shorter adsorbates in both series disrupts interchain vdW interactions, leading to gauche defects in the long-chain adsorbates (**AM-C15-DT** and **TMA-C15-DT**) of the mixed SAMs. In addition, the longer chain spacers likely form fluidlike structures in these SAMs, with the long alkyl chains either twisted or lying somewhat parallel to the surface.[40]

https://dx.doi.org/10.1021/acsanm.0c01059
ACS Appl. Nano Mater. 2020, 3, 6621−6628

Oligonucleotide Conjugation on Binary SAMs Derived from Ammonium and Trimethylammonium Bidentate Adsorbates. *Oligonucleotide Conjugation: Analysis of Film Thickness.* To probe the conjugation of oligonucleotides, the thicknesses of the SAMs were obtained before and after incubation with single-stranded DNA as described previously.[26] The results in Table 2 show that the thicknesses of the SAMs increase after conjugation with the oligonucleotides, except for the film generated from **ODT**. In contrast to the **ODT** SAMs, the SAMs derived from the ammonium-terminated and/or trimethylammonium-terminated adsorbates provide a platform for the electrostatic interaction with the phosphate backbones of the oligonucleotides. After incubation, the increase in film thickness of the **AM** series was 4, 8, 5, 3, and 2 Å for **AM-C15-DT** (1.00), **AM-C15-DT** (0.75), **AM-C15-DT** (0.50), **AM-C15-DT** (0.25), and **TMA-C6-DT** (1.0), respectively. Separately, for the **TMA** series, the increase in film thickness after incubation with oligonucleotides was 4, 8, 6, 5, and 2 Å for **TMA-C15-DT** (1.0), **TMA-C15-DT** (0.75), **TMA-C15-DT** (0.50), **TMA-C15-DT** (0.25), and **AM-C6-DT** (1.0), respectively. Notably, the highest change in thickness was observed for the 75:25 molar ratio in both the **AM** and **TMA** series (8 Å), with the other concentrations exhibiting smaller increases in thicknesses. The incorporation of the shorter **TMA-C6-DT** and **AM-C6-DT** adsorbates into the **AM** and **TMA** series, respectively, likely forms a densely packed molecular layer near the gold surface and a loosely packed upper layer, allowing the oligonucleotides to intercalate into the SAMs. Further quantitative analysis in the following sections provides additional insight into the performance of both of the mixed SAM series.

Table 2. Film Thickness Measurements for SAMs Derived from ODT, the AM Series (AM-C15-DT/TMA-C6-DT), and the TMA Series (TMA-C15-DT/AM-C6-DT) After Conjugation with Oligonucleotides[a]

after conjugation with oligonucleotide **AM** series			after conjugation with oligonucleotide **TMA** series		
adsorbate	T^b(Å)	ΔT^c (Å)	adsorbate	T^b(Å)	ΔT^c (Å)
ODT	23 ± 1		**ODT**	23 ± 1	
AM-C15-DT (1.0)	25 ± 1	4	**TMA-C15-DT** (1.0)	26 ± 1	4
AM-C15-DT (0.75)	27 ± 1	8	**TMA-C15-DT** (0.75)	28 ± 1	8
AM-C15-DT (0.50)	21 ± 1	5	**TMA-C15-DT** (0.50)	23 ± 1	6
AM-C15-DT (0.25)	19 ± 1	3	**TMA-C15-DT** (0.25)	21 ± 1	5
TMA-C6-DT (1.0)	16 ± 1	2	**AM-C6-DT** (1.0)	15 ± 1	2

[a]The solution mole fraction of the adsorbate is denoted inside the parentheses. [b]T indicates film thickness after conjugation with oligonucleotides. [c]ΔT indicates the difference between film thicknesses before and after conjugation with oligonucleotides.

Oligonucleotide Conjugation: Analysis by XPS. We used XPS to provide a more detailed understanding of oligonucleotide immobilization on the surface of the binary SAMs after incubation with oligonucleotides.[41,49] Spectra were obtained in the C 1s, N 1s, and P 2p regions to probe for the presence of signature peaks characteristic of the oligonucleotides. The XPS spectra for the **AM** and **TMA** series after incubation with the oligonucleotides are shown in Figure 4. The C 1s region (Figure 4a1,b1) indicates the presence of the C−O, C−N, and C−C species at ∼286.6, ∼286, and 285 eV, respectively, consistent with the molecular composition of the adsorbates in these SAMs. Analysis of the N 1s region of both SAM series (Figure 4a2,b2) exhibits a new peak in the ∼398−401 eV region, compared to the original spectra shown in Figure 2, except for the **ODT** SAM. The appearance of this peak is indicative of the nitrogen present in the purine and pyrimidine of the nitrogenous bases of single-stranded DNA.[41] Further, probing of the P 2p region revealed a peak at ∼134 eV (Figure 4a3,b3) for both the **AM** and **TMA** series originating from the phosphate backbones of the oligonucleotides.[41] Moreover, the lack of signature oligonucleotide peaks in the XPS spectra of the SAM derived from **ODT** validates the ability of the charged terminal species in the **AM** and **TMA** SAMs to provide a binding platform for electrostatic interactions between the positively charged ammonium tailgroups and the negatively charged phosphate backbones of the oligonucleotides.

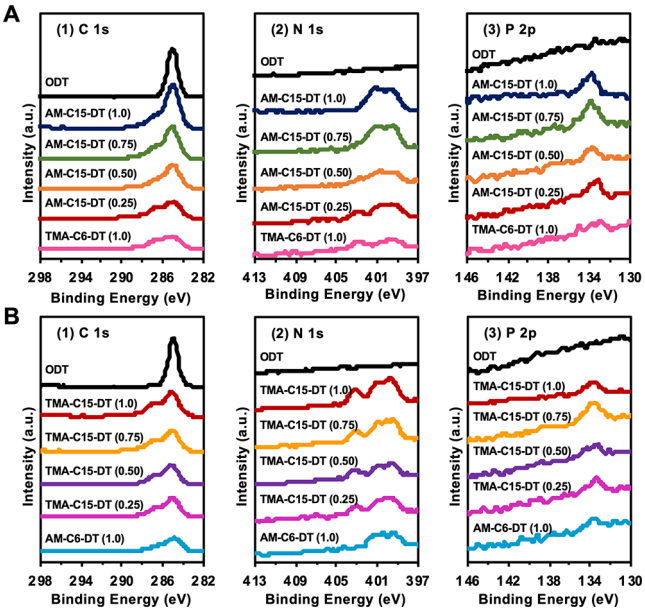

Figure 4. XPS spectra of the (A) **AM** series and (B) **TMA** series after incubation with oligonucleotides in the (1) C 1s, (2) N 2p, and (3) P 2p regions. SAMs derived from **ODT** are included in both panels for comparison.

To analyze in greater detail the degree of conjugation between the SAMs and the oligonucleotides, the P/Au ratios were determined and are shown in Table S5. For the **AM** series, the P/Au ratio decreases in the following order: **AM-C15-DT** (0.75) > **AM-C15-DT** (0.50) > **AM-C15-DT** (1.0) > **AM-C15-DT** (0.25) > **TMA-C6-DT** (1.0). For the **TMA** series, the P/Au ratio decreases as follows: **TMA-C15-DT** (0.75) > **TMA-C15-DT** (0.50) > **TMA-C15-DT** (0.25) > **TMA-C15-DT** (1.0) > **AM-C6-DT** (1.0). The trends observed in the P/Au ratios are in congruence with the changes in thickness observed for the respective SAMs after incubation with the oligonucleotides. Taking the thickness data as well as the P/Au ratios, the binary SAMs derived from **AM-C15-DT** (0.75) and **TMA-C15-DT** (0.75) exhibited the greatest amount of oligonucleotide conjugation. To quantify the amount of conjugated oligonucleotides, the **AM-C15-DT** (0.75) and **TMA-C15-DT** (0.75) SAMs and the correspond-

https://dx.doi.org/10.1021/acsanm.0c01059
ACS Appl. Nano Mater. 2020, 3, 6621−6628

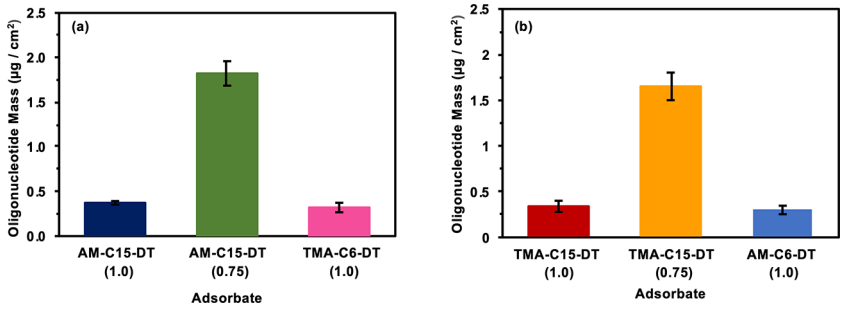

Figure 5. Mass loadings of oligonucleotides for (a) the **AM** series and (b) the **TMA** series.

ing single-component SAMs were further analyzed by EQCM as described below.

Oligonucleotide Conjugation: Mass Loading Analysis by Electrochemical Quartz Crystal Microbalance (EQCM). Analysis by electrochemical quartz crystal microbalance (EQCM) was performed to quantify the amount of oligonucleotides present within and/or on the monolayer surfaces. The generated SAMs were analyzed by EQCM both prior to and after conjugation with the oligonucleotides. Initial studies focused on the mass change associated with SAM formation, where the changes in frequency shown in Figure S8 and the changes in mass shown in Figure S9 were determined using the Sauerbrey equation (eq 1)[50,51]

$$-\Delta F = C_f \times \Delta M \quad (1)$$

Here, ΔF denotes the difference in the frequency of the bare QCM crystal before and after SAM formation. The sensitivity of the crystal is represented by C_f, 226 μg^{-1} cm^{-2}, which is provided by the manufacturer of the QCM crystal. Once the SAMs were formed, we used the same methodology to determine the amounts of surface-immobilized oligonucleotides, where ΔF corresponds to the change in frequency of the SAM before and after incubation with the oligonucleotides (see Figure S10). The corresponding amount (μg) of immobilized oligonucleotides is shown in Figure 5a,b. In the **AM** series, the amounts of oligonucleotides were observed to decrease as follows: **AM-C15-DT** (0.75) > **AM-C15-DT** (1.0) > **TMA-C6-DT** (1.0), with mass values of 1.82, 0.37, and 0.32 μg, respectively. Similarly, the amounts of oligonucleotides determined for the **TMA** series were observed to decrease as follows: **TMA-C15-DT** (0.75) > **TMA-C15-DT** (1.0) > **AM-C6-DT** (1.0), with mass values of 1.65, 0.34, and 0.30 μg, respectively. The mass changes based on the EQCM data are consistent with the P 2p/Au 4f results (see Table S5). It is important to note that the **AM-C15-DT** (0.75) SAMs and the **TMA-C15-DT** (0.75) SAMs exhibited the highest oligonucleotide surface loading capacity out of the two series. This result likely arises from having the sterically bulky ammonium termini of the **TMA-C6-DT** and **AM-C6-DT** adsorbates buried close to the surface of gold in these binary SAMs, which can plausibly give rise to large positively charged cavities for oligonucleotide binding.

With regard to our previous studies of oligonucleotide loading, SAMs derived from the mixtures of bidentate adsorbates bearing trimethylammonium and triethylammonium termini exhibited a higher loading capacity than the surfaces examined here (i.e., a maximum of 2.15 $\mu g/cm^2$ for the previous SAMs vs a maximum of 1.82 $\mu g/cm^2$ for the current SAMs).[26] Interestingly, studies of similarly structured SAMs characterized by contact angle measurements using the polar protic solvent water showed that ammonium-terminated SAMs exhibit higher surface tension than quaternary ammonium-terminated SAMs;[23,24] however, the fact that the oligonucleotide loadings in Figure 5a are parallel to those in Figure 5b suggests that any differences in electrostatic repulsion and/or hydrogen bonding within the ammonium and trimethylammonium headgroups are insignificant when it comes to oligonucleotide loading. In contrast, when compared to our previous study,[26] the maximum oligonucleotide binding occurred with SAMs that were more loosely packed than those in the present study (i.e., 36 vs 44% chain packing density, respectively, relative to *n*-octadecanethiol SAMs), which emphasizes the important role of loose chain packing enabled by our bidentate adsorbates for oligonucleotide delivery.

CONCLUSIONS

Two series of binary SAMs composed of ammonium and trimethylammonium-terminated bidentate adsorbates were studied in an effort to develop a high-capacity nanoscale platform for the loading and delivery of oligonucleotides. The effect of burying the ammonium or trimethylammonium moiety into the film was examined by introducing a short-chain adsorbate, **TMA-C6-DT** in the **AM** series and **AM-C6-DT** in the **TMA** series, into SAMs comprising complementary long-chain adsorbates. By systematically adjusting the concentration of the shorter adsorbate in both series, we were able to determine the ideal composition corresponding to the maximum amount of oligonucleotide loading. Analysis of the SAMs by ellipsometry, PM-IRRAS, XPS, and EQCM revealed that the 75:25 ratio (75% long adsorbate, 25% short adsorbate) gave the maximum amount of oligonucleotide loading in both the **AM** and **TMA** series. These studies lay the groundwork for designing light-triggerable Au nanoparticle-based delivery vehicles for gene therapy that can elude the degradation of oligonucleotides.

ASSOCIATED CONTENT

Supporting Information

The Supporting Information is available free of charge at https://pubs.acs.org/doi/10.1021/acsanm.0c01059.

Materials, methods, synthetic procedures, characterization data (^1H and ^{13}C NMR spectra; mass spectrometry) for **AM-C15-DT**, **AM-C6-DT**, **TMA-C15-DT**, and **TMA-C6-DT**; additional XPS spectra and EQCM data, and details of the conjugation of the SAMs with ssDNA (PDF)

https://dx.doi.org/10.1021/acsanm.0c01059
ACS Appl. Nano Mater. 2020, 3, 6621−6628

AUTHOR INFORMATION

Corresponding Authors

Preethi H. Gunaratne − *Department of Biology and Biochemistry, University of Houston, Houston, Texas 77204-5001, United States*; Email: phgunaratne@uh.edu

T. Randall Lee − *Departments of Chemistry and Chemical Engineering and the Texas Center for Superconductivity, University of Houston, Houston, Texas 77204-5003, United States*; orcid.org/0000-0001-9584-8861; Email: trlee@uh.edu

Authors

Johnson Hoang − *Department of Biology and Biochemistry, University of Houston, Houston, Texas 77204-5001, United States*

Chul Soon Park − *Departments of Chemistry and Chemical Engineering and the Texas Center for Superconductivity, University of Houston, Houston, Texas 77204-5003, United States*

Maria D. Marquez − *Departments of Chemistry and Chemical Engineering and the Texas Center for Superconductivity, University of Houston, Houston, Texas 77204-5003, United States*

Complete contact information is available at: https://pubs.acs.org/10.1021/acsanm.0c01059

Notes

The authors declare no competing financial interest.

ACKNOWLEDGMENTS

The National Science Foundation (CHE-1710561, T.R.L.), the Robert A. Welch Foundation (grant no. E-1320, T.R.L.), the Texas Center for Superconductivity at the University of Houston (T.R.L.), and the Cancer Prevention and Research Institute of Texas (RP110355, P.H.G.) provided generous financial support for this research.

REFERENCES

(1) Charles, P. T.; Vora, G. J.; Andreadis, J. D.; Fortney, A. J.; Meador, C. E.; Dulcey, C. S.; Stenger, D. A. Fabrication and Surface Characterization of DNA Microarrays Using Amine- and Thiol-Terminated Oligonucleotide Probes. *Langmuir* **2003**, *19*, 1586−1591.

(2) Asiaei, S.; Nieva, P.; Vijayan, M. M. Fast Kinetics of Thiolic Self-Assembled Monolayer Adsorption on Gold: Modeling and Confirmation by Protein Binding. *J. Phys. Chem. B* **2014**, *118*, 13697−13703.

(3) Min, H.; Girard-Lauriault, P.-L.; Gross, T.; Lippitz, A.; Dietrich, P.; Unger, W. E. S. Ambient-Ageing Processes in Amine Self-Assembled Monolayers on Microarray Slides as Studied by ToF-SIMS with Principal Component Analysis, XPS, and NEXAFS Spectroscopy. *Anal. Bioanal. Chem.* **2012**, *403*, 613−623.

(4) Jang, L.-S.; Keng, H.-K. Modified Fabrication Process of Protein Chips Using a Short-Chain Self-Assembled Monolayer. *Biomed. Microdevices* **2008**, *10*, 203−211.

(5) Graf, N.; Gross, T.; Wirth, T.; Weigel, W.; Unger, W. E. S. Application of XPS and ToF-SIMS for Surface Chemical Analysis of DNA Microarrays and their Substrates. *Anal. Bioanal. Chem.* **2009**, *393*, 1907−1912.

(6) Love, J. C.; Estroff, L. A.; Kriebel, J. K.; Nuzzo, R. G.; Whitesides, G. M. Self-Assembled Monolayers of Thiolates on Metals as a Form of Nanotechnology. *Chem. Rev.* **2005**, *105*, 1103−1170.

(7) Nicosia, C.; Huskens, J. Reactive Self-Assembled Monolayers: from Surface Functionalization to Gradient Formation. *Mater. Horiz.* **2014**, *1*, 32−45.

(8) Wadu-Mesthrige, K.; Amro, N. A.; Liu, G.-Y. Immobilization of Proteins on Self-Assembled Monolayers. *Scanning* **2006**, *22*, 380−388.

(9) Kao, W.-L.; Chang, H.-Y.; Yen, G.-J.; Kuo, D.-Y.; You, Y.-W.; Huang, C.-C.; Kuo, Y.-T.; Lin, J.-H.; Shyue, J.-J. Adsorption Behavior of Plasmid DNA on Binary Self-Assembled Monolayers Modified Gold Substrates. *J. Colloid Interface Sci.* **2012**, *382*, 97−104.

(10) Lin, Y.-C.; Yu, B.-Y.; Lin, W.-C.; Lee, S.-H.; Kuo, C.-H.; Shyue, J.-J. Tailoring the Surface Potential of Gold Nanoparticles with Self-Assembled Monolayers with Mixed Functional Groups. *J. Colloid Interface Sci.* **2009**, *340*, 126−130.

(11) Tatiparti, K.; Sau, S.; Kashaw, S. K.; Iyer, A. K. siRNA Delivery Strategies: A Comprehensive Review of Recent Developments. *Nanomaterials* **2017**, *7*, No. 77.

(12) Whitehead, K. A.; Langer, R.; Anderson, D. G. Knocking Down Barriers: Advances in siRNA Delivery. *Nat. Rev. Drug Discovery* **2009**, *8*, 129−138.

(13) Mukherjee, S.; Sengupta, K.; Das, M. R.; Jana, S. S.; Dey, A. Site-Specific Covalent Attachment of Heme Proteins on Self-Assembled Monolayers. *JBIC, J. Biol. Inorg. Chem.* **2012**, *17*, 1009−1023.

(14) Li, L.; Chen, S.; Jiang, S. Protein Adsorption on Alkanethiolate Self-Assembled Monolayers: Nanoscale Surface Structural and Chemical Effects. *Langmuir* **2003**, *19*, 2974−2982.

(15) Baumann, V.; Winkler, J. miRNA-Based Therapies: Strategies and Delivery Platforms for Oligonucleotide and Non-Oligonucleotide Agents. *Future Med. Chem.* **2014**, *6*, 1967−1984.

(16) Jackson, A. L.; Burchard, J.; Leake, D.; Reynolds, A.; Schelter, J.; Guo, J.; Johnson, J. M.; Lim, L.; Karpilow, J.; Nichols, K.; Marshall, W.; Khvorova, A.; Linsley, P. S. Position-Specific Chemical Modification of siRNAs Reduces "Off-Target" Transcript Silencing. *RNA* **2006**, *12*, 1197−1205.

(17) Lee, M.-Y.; Park, S.-J.; Park, K.; Kim, K. S.; Lee, H.; Hahn, S. K. Target-Specific Gene Silencing of Layer-by-Layer Assembled Gold−Cysteamine/siRNA/PEI/HA Nanocomplex. *ACS Nano* **2011**, *5*, 6138−6147.

(18) Rana, S.; Bajaj, A.; Mout, R.; Rotello, V. M. Monolayer Coated Gold Nanoparticles for Delivery Applications. *Adv. Drug Delivery Rev.* **2012**, *64*, 200−216.

(19) Chang, H.-Y.; You, Y.-W.; Liao, H.-Y.; Shyue, J.-J. Binary Self-Assembled Monolayers Modified Au Nanoparticles as Carriers in Biological Applications. *Biointerphases* **2014**, *9*, No. 041005.

(20) Wu, J.; Wang, H.; Zhu, A.; Long, F. Adsorption Kinetics of Single-Stranded DNA on Functional Silica Surfaces and Its Influence Factors: An Evanescent-Wave Biosensor Study. *ACS Omega* **2018**, *3*, 5605−5614.

(21) Callari, F. L.; Petralia, S.; Conoci, S.; Sortino, S. Light-Triggered DNA Release by Dynamic Monolayer Films. *New J. Chem.* **2008**, *32*, 1899−1903.

(22) Ah Qune, L. F. N.; Makino, K.; Tamada, K.; Chen, W.; Wee, A. T. S. Selective Adsorption of l-Tartaric Acid on Gemini-Type Self-Assembled Monolayers. *J. Phys. Chem. C* **2008**, *112*, 3049−3053.

(23) Kim, S. T.; Saha, K.; Kim, C.; Rotello, V. M. The Role of Surface Functionality in Determining Nanoparticle Cytotoxicity. *Acc. Chem. Res.* **2013**, *46*, 681−691.

(24) Lee, S. H.; Bae, K. H.; Kim, S. H.; Lee, K. R.; Park, T. G. Amine-Functionalized Gold Nanoparticles as Non-Cytotoxic and Efficient Intracellular siRNA Delivery Carriers. *Int. J. Pharm.* **2008**, *364*, 94−101.

(25) Lee, H. J.; Jamison, A. C.; Lee, T. R. Boc-Protected ω-Amino Alkanedithiols Provide Chemically and Thermally Stable Amine-Terminated Monolayers on Gold. *Langmuir* **2015**, *31*, 2136−2146.

(26) Hoang, J.; Park, C. S.; Lee, H. J.; Marquez, M. D.; Zenasni, O.; Gunaratne, P. H.; Lee, T. R. Quaternary Ammonium-Terminated Films Formed from Mixed Bidentate Adsorbates Provide a High-Capacity Platform for Oligonucleotide Delivery. *ACS Appl. Mater. Interfaces* **2018**, *10*, 40890−40900.

(27) Filip, J.; Popelka, A.; Bertok, T.; Holazova, A.; Osicka, J.; Kollar, J.; Ilcikova, M.; Tkac, J.; Kasak, P. pH-Switchable Interaction

of a Carboxybetaine Ester-Based SAM with DNA and Gold Nanoparticles. *Langmuir* **2017**, *33*, 6657−6666.
(28) Honarvarfard, E.; Gamella, M.; Guz, N.; Katz, E. Electrochemically-Controlled DNA Release under Physiological Conditions from a Monolayer-Modified Electrode. *Electroanalysis* **2017**, *29*, 324−329.
(29) Bansal, M. DNA Structure: Revisiting the Watson−Crick Double Helix. *Curr. Sci.* **2003**, *85*, 1556−1563.
(30) Goodman, C. M.; Chari, N. S.; Han, G.; Hong, R.; Ghosh, P.; Rotello, V. M. DNA-Binding by Functionalized Gold Nanoparticles: Mechanism and Structural Requirements. *Chem. Biol. Drug Des.* **2006**, *67*, 297−304.
(31) Park, C. S.; Lee, H. J.; Jamison, A. C.; Lee, T. R. Robust Thick Polymer Brushes Grafted from Gold Surfaces Using Bidentate Thiol-Based Atom-Transfer Radical Polymerization Initiators. *ACS Appl. Mater. Interfaces* **2016**, *8*, 5586−5594.
(32) Lee, H. J.; Jamison, A. C.; Lee, T. R. Two Are Better than One: Bidentate Adsorbates Offer Precise Control of Interfacial Composition and Properties. *Chem. Mater.* **2016**, *28*, 5356−5364.
(33) Durymanov, M.; Reineke, J. Non-viral Delivery of Nucleic Acids: Insight Into Mechanisms of Overcoming Intracellular Barriers. *Front. Pharmacol.* **2018**, *9*, No. 971.
(34) Bus, T.; Traeger, A.; Schubert, U. S. The Great Escape: How Cationic Polyplexes Overcome the Endosomal Barrier. *J. Mater. Chem. B* **2018**, *6*, 6904−6918.
(35) Ding, Y.; Jiang, Z.; Saha, K.; Kim, C. S.; Kim, S. T.; Landis, R. F.; Rotello, V. M. Gold Nanoparticles for Nucleic Acid Delivery. *Mol. Ther.* **2014**, *22*, 1075−1083.
(36) Benjaminsen, R. V.; Mattebjerg, M. A.; Henriksen, J. R.; Moghimi, S. M.; Andresen, T. L. The Possible "Proton Sponge" Effect of Polyethylenimine (PEI) Does Not Include Change in Lysosomal pH. *Mol. Ther.* **2013**, *21*, 149−157.
(37) Conde, J.; Ambrosone, A.; Hernandez, Y.; Tian, F.; McCully, M.; Berry, C. C.; Baptista, P. V.; Tortiglione, C.; de la Fuente, J. M. 15 Years on siRNA Delivery: Beyond the State-of-the-Art on Inorganic Nanoparticles for RNAi Therapeutics. *Nano Today* **2015**, *10*, 421−450.
(38) Erbaş, A.; de la Cruz, M. O.; Marko, J. F. Effects of Electrostatic Interactions on Ligand Dissociation Kinetics. *Phys. Rev. E* **2018**, *97*, No. 022405.
(39) Zhai, X.; Lee, H. J.; Tian, T.; Lee, T. R.; Garno, J. C. Nanoscale Lithography Mediated by Surface Self-Assembly of 16-[3,5-Bis-(mercaptomethyl)phenoxy]hexadecanoic Acid on Au(111) Investigated by Scanning Probe Microscopy. *Molecules* **2014**, *19*, 13010−13026.
(40) Bain, C. D.; Whitesides, G. M. Modeling Organic Surfaces with Self-Assembled Monolayers. *Adv. Mater.* **1989**, *1*, 110−116.
(41) Ptasińska, S.; Stypczyńska, A.; Nixon, T.; Mason, N. J.; Klyachko, D. V.; Sanche, L. X-ray Induced Damage in DNA Monitored by X-Ray Photoelectron Spectroscopy. *J. Chem. Phys.* **2008**, *129*, No. 065102.
(42) Baio, J. E.; Weidner, T.; Brison, J.; Graham, D. J.; Gamble, L. J.; Castner, D. G. Amine Terminated SAMs: Investigating Why Oxygen is Present in these Films. *J. Electron Spectrosc. Relat. Phenom.* **2009**, *172*, 2−8.
(43) Castner, D. G.; Hinds, K.; Grainger, D. W. X-ray Photoelectron Spectroscopy Sulfur 2p Study of Organic Thiol and Disulfide Binding Interactions with Gold Surfaces. *Langmuir* **1996**, *12*, 5083−5086.
(44) Lee, H. J.; Jamison, A. C.; Yuan, Y.; Li, C.-H.; Rittikulsittichai, S.; Rusakova, I.; Lee, T. R. Robust Carboxylic Acid-Terminated Organic Thin Films and Nanoparticle Protectants Generated from Bidentate Alkanethiols. *Langmuir* **2013**, *29*, 10432−10439.
(45) Vericat, C.; Vela, M. E.; Corthey, G.; Pensa, E.; Cortés, E.; Fonticelli, M. H.; Ibanez, F.; Benitez, G. E.; Carro, P.; Salvarezza, R. Self-Assembled Monolayers of Thiolates on Metals: A Review Article on Sulfur-Metal Chemistry and Surface Structures. *RSC Adv.* **2014**, *4*, 27730−27754.
(46) Park, J.-S.; Vo, A. N.; Barriet, D.; Shon, Y.-S.; Lee, T. R. Systematic Control of the Packing Density of Self-Assembled Monolayers Using Bidentate and Tridentate Chelating Alkanethiols. *Langmuir* **2005**, *21*, 2902−2911.
(47) Allara, D. L.; Nuzzo, R. G. Spontaneously Organized Molecular Assemblies. 1. Formation, Dynamics, and Physical Properties of n-Alkanoic Acids Adsorbed from Solution on an Oxidized Aluminum Surface. *Langmuir* **1985**, *1*, 45−52.
(48) Snyder, R. G.; Strauss, H. L.; Elliger, C. A. Carbon-Hydrogen Stretching Modes and the Structure of n-Alkyl Chains. 1. Long, Disordered Chains. *J. Phys. Chem. A* **1982**, *86*, 5145−5150.
(49) Lee, C.-Y.; Gong, P.; Harbers, G. M.; Grainger, D. W.; Castner, D. G.; Gamble, L. J. Surface Coverage and Structure of Mixed DNA/Alkylthiol Monolayers on Gold: Characterization by XPS, NEXAFS, and Fluorescence Intensity Measurements. *Anal. Chem.* **2006**, *78*, 3326−3334.
(50) Lederer, T.; Stehrer, B. P.; Bauer, S.; Jakoby, B.; Hilber, W. Utilizing a High Fundamental Frequency Quartz Crystal Resonator as a Biosensor in a Digital Microfluidic Platform. *Sens. Actuators, A* **2011**, *172*, 161−168.
(51) Vashist, S. K.; Vashist, P. Recent Advances in Quartz Crystal Microbalance-Based Sensors. *J. Sens.* **2011**, *2011*, No. 571405.

https://dx.doi.org/10.1021/acsanm.0c01059
ACS Appl. Nano Mater. 2020, 3, 6621−6628